View metadata, citation and similar papers at core.ac.uk
brought to you by CORE
provided by Caltech Authors - Main

Supplementary Information:

Tunable Large Resonant Absorption in a Mid-Infrared Graphene Salisbury Screen

Min Seok Jang[1, †], Victor W. Brar[2,3, †], Michelle C. Sherrott[2], Josue J. Lopez[2], Laura B. Kim[2], Seyoon Kim[2], Mansoo Choi[1,4], and Harry A. Atwater[2,3]

† These authors contributed equally.

1) Global Frontier Center for Multiscale Energy Systems, Seoul National University, Seoul 151-747, Republic of Korea

2) Thomas J. Watson Laboratory of Applied Physics, California Institute of Technology, Pasadena, CA 91125

3) Kavli Nanoscience Institute, California Institute of Technology, Pasadena, CA91125

4) Division of WCU Multiscale Mechanical Design, School of Mechanical and Aerospace Engineering, Seoul National University, Seoul 151-742

I. Device Fabrication

SiN_x membranes were obtained commercially from Norcada, part #NX10500F. Electron beam lithography at 100keV is used to pattern nanoresonator arrays in PMMA spun coated onto the devices, and the pattern is transferred to the graphene via an oxygen plasma etch. Our resonators have widths varying from 20 – 60nm, with 9:1 aspect ratios and a pitch of 2-2.5 times the width. The resonators are spanned perpendicularly by graphene crossbars of a width equal to the nanoresonator width. This aids conductivity across the patterned arrays despite occasional cracks and domain boundaries in the CVD graphene sheet.

II. Electromagnetic Simulations

We solve Maxwell's equation by using finite element method. Graphene is modeled as a thin layer of the thickness τ and impose the relative permittivity $\epsilon_G = 1 + i\sigma/(\epsilon_0\omega\tau)$. In actual calculation, τ is chosen to be 0.1 nm which shows good convergence with respect to the $\tau \to 0$ limit as seen in Figure S1. The complex optical conductivity of graphene $\sigma(\omega)$ is evaluated within local random phase approximation.[1]

$$\sigma(\omega) = \frac{2ie^2T}{\pi\hbar(\omega + i\Gamma)}\log\left[2\cosh\left(\frac{E_F}{2T}\right)\right] + \frac{e^2}{4\hbar}\left[H\left(\frac{\omega}{2}\right) + \frac{4i\omega}{\pi}\int_0^\infty d\eta\,\frac{H(\eta) - H\left(\frac{\omega}{2}\right)}{\omega^2 - 4\eta^2}\right.,$$

where

$$H(\eta) = \frac{\sinh(\eta/T)}{\cosh(E_F/T) + \cosh(\eta/T)}.$$

Here, the temperature T is set as 300K. The intraband scattering rate Γ takes into account scattering by impurities Γ_{imp} and by optical phonons Γ_{oph}. By analyzing the absorption peak width when the resonance energy is much lower than the graphene optical phonon energy (~1600cm^{-1}), the impurity scattering rate can be approximated to be $\Gamma_{\mathrm{imp}} = ev_F/\mu\sqrt{n\pi}$ with the mobility $\mu = 550\mathrm{cm}^2/\mathrm{Vs}$.[2] The rate of optical phonon scattering is estimated from theoretically obtained self-energy $\Sigma_{\mathrm{oph}}(\omega)$, as $\Gamma_{\mathrm{oph}}(\omega) = 2\mathrm{Im}\left[\Sigma_{\mathrm{oph}}(\omega)\right]$.[2-4] The frequency dependent

dielectric functions of Au and SiN_x are taken from Palik [5] and Cataldo et al. [6], respectively. Finally, a constant factor, which accounts for experimental imperfections such as dead resonators in the actual device, is multiplied to the simulated spectra. This degradation factor is determined to be 0.72 by comparing simulation and measurement. Figure S2 shows that the resulting theoretical absorption spectra reproduce quite well the experimental data.

III. Determination of Carrier Density

The carrier density of the nanoresonators was determined by fitting the peak frequencies of the simulated absorption spectra to the experimentally measured absorption peaks of resonators fabricated with different widths. The resulting carrier density values are comparable to those calculated using a simple parallel plate capacitor model with a 1 μm thick SiN_x dielectric, as shown in Figure S3a, yet there is some deviation. We can attribute the discrepancies to a number of possible effects. First, our SiN_x membranes were obtained from a commercial supplier (Norcada) and their stoichiometry and resulting DC dielectric constant, κ, is not precisely known. This allows for a range of possible values for κ, which can lead to significant differences in the induced carrier density in a graphene device. Second, our measurements were performed under FTIR purge gas (free of H_2O and CO_2), but atmospheric impurities were likely still present during the measurements. Those types of impurities have previously been shown to induce hysteresis effects in the conductance curves of graphene FET devices,[7-10] and we observe similar behavior in our devices, as shown in Figure S3b. Because the concentration of those impurities can depend on the applied gate bias, they can also alter the carrier density vs. gate bias curves, and in Figure S3a we have included a theoretical estimate of those effects.[9] In addition to atmospheric impurities, the SiN_x surface itself can contain charge traps that fill or empty with the applied gate bias. Such charge traps could induce anomalous behavior in the conductance curves of the graphene FET devices, similar to what has been observed in the presence of metallic impurities.[11] Finally, we note that we have removed some of the graphene surface area in the process of fabricating the nanoresonators. This difference in total available surface area should alter the carrier density dependence assumed by the capacitor model, such that more charge is likely packed into a smaller area. In Figure S3a we have

provided a simple estimate of this effect based on the assumption that an equal amount of induced carriers are distributed equally across the smaller available surface area, leading to larger carrier densities. However, theoretical predictions have shown that the extra carrier density should preferably accumulate on the edges of the graphene nanoresonators, and thus alter their plasmonic resonances in more sophisticated ways.[12]

IV. Peak Width Analysis

In Figure S4a, we plot the full with at half maximum (FWHM) of the absorption peaks of graphene nanoresonator arrays with various sizes and doping levels. The linewidth, which can be interpreted as the plasmon scattering rate, almost monotonically increases with increasing resonance frequency and decreasing resonator width. The lifetime of plasmon is estimated as 10-50 fs from inverse linewidth.

When the substrate medium is lossless and dispersionless, the scattering rate of graphene plasmon is simply equal to the electron scattering rate. However, in our sample, the interaction with SiN_x substrate polar phonons results in a deviation of the plasmon scattering rate from the electron scattering rate. Therefore, we extract the intraband electron scattering rate (Γ) by fitting the FWHM of the simulated spectrum to the measured plasmon linewidth, as shown in figure S4b.

We found that there is no noticeable difference in the electron scattering rates among nanoresoantors wider than 40nm. Because those nanoresonators oscillate at frequencies much lower than graphene optical phonon (~1600cm^{-1}), the dominant damping mechanism in this regime is scattering from impurities.[2,3] The average carrier mobility μ, converted from the electron scattering rate via $\mu = ev_F/\Gamma\sqrt{n\pi}$, is determined as 550cm^2/Vs with standard deviation 50cm^2/Vs. On the other hand, at frequencies higher than 1600cm^{-1}, the electron scattering rate of 20nm nanoresonators dramatically increases as the carrier density increases (and thus the plasmon frequency increases), possibly due to coupling with graphene optical phonons.

V. Derivation of Surface Admittance of a Thin Layer

Consider a thin layer of thickness τ and admittance Y_{GR} sitting atop a dielectric with thickness d and admittance $Y_{\mathrm{SiN_x}}$ deposited on a reflecting mirror as diagramed in the inset of Figure 1a. For normally incident light, the effective surface admittance of the stack is given by [13,14]

$$Y = Y_{\mathrm{GR}} \frac{Y'_{\mathrm{SiN_x}} - iY_{\mathrm{GR}} \tan(k_1\tau)}{Y_{\mathrm{GR}} - iY'_{\mathrm{SiN_x}} \tan(k_1\tau)},$$

where $Y_{\mathrm{GR}} = \sqrt{\epsilon_{\mathrm{GR}}/\mu_{\mathrm{GR}}}$ and $k_1 = \omega\sqrt{\epsilon_{\mathrm{GR}}\mu_{\mathrm{GR}}}$ are the wave admittance and the wavevector inside the thin sheet, respectively. $Y'_{\mathrm{SiN_x}}$ is the effective admittance of the dielectric as viewed from the position of the sheet, and is given by $Y'_{\mathrm{SiN_x}} = Y_{\mathrm{SiN_x}} \cot(k_2 d)$, where k_2 is the wavevector inside the SiN_x layer. For frequencies such that $d = m\lambda/4$ and for $k_1\tau \ll 1$, then $Y'_{\mathrm{SiN_x}} \ll Y_{\mathrm{GR}}$ and $\tan(k_1\tau) \to k_1\tau$, and the above equation reduces to $Y = -i\omega\varepsilon\tau$.

VI. Calculation of Surface Admittance of Graphene Nanoresonator Arrays

The surface admittance $Y = -i\omega\varepsilon\tau$ of a graphene nanoresonator array is equivalent to its effective sheet conductivity σ_{eff}, which can be evaluated from the far-field transmission and reflection coefficients. Consider a homogeneous thin film of conductivity σ_{eff} placed on the interface ($z = 0$) between air ($z < 0$) and SiN_x ($z > 0$) and a plane wave polarized along x direction is normally incident on the surface. The surface parallel electric field is continuous $E_x^{0+} = E_x^{0-}$ at the interface, while the magnetic fields are discontinuous due to the surface current, $H_y^{0+} - H_y^{0-} = \sigma_{\mathrm{eff}} E_x(z = 0) = YE_x(z = 0)$. From these boundary conditions, the transmission (t) and reflection (r) coefficients satisfy the following equations,

$$1 + r = t,$$
$$(1 - r) - n_{\mathrm{SiN_x}} t = \left(\frac{Y}{Y_0}\right) t,$$

where $n_{\mathrm{SiN_x}}$ is the refractive index of $\mathrm{SiN_x}$. The normalized surface admittance Y/Y_0 is then solely written in terms of transmission coefficient,

$$\frac{Y}{Y_0} = \frac{2}{t} - 1 - n_{\mathrm{SiN_x}}.$$

Because the fields of graphene plasmons are tightly confined near the surface with characteristic decay length similar to the width of the nanoresonators, we record the electric field of the transmitted wave at a position sufficiently far from the surface ($z_0 = 1\mathrm{um}$) in order to exclude the evanescent field of graphene plasmons. The far field transmission coefficient is then obtained by accounting for the propagation factor

$$t = \frac{E_{\mathrm{x}}(z_0)\exp[-in_{\mathrm{SiN_x}}k_0 z_0\,]}{E_0(0)},$$

where E_0 is the electric field of incident wave at the surface.

Figure S5 plots the resulting complex surface admittance of a graphene nanoribbon array as a function of frequency. As in figure 4, both ribbon width and the spacing between the ribbons are set as 40nm. On resonance, $\mathrm{Im}[Y]$ crosses zero, while $\mathrm{Re}[Y]$, which is directly proportional to the absorption cross section σ_{Abs} of individual resonator, has its maximum. As graphene becomes less lossy, the plasmon resonance gets sharper and stronger.

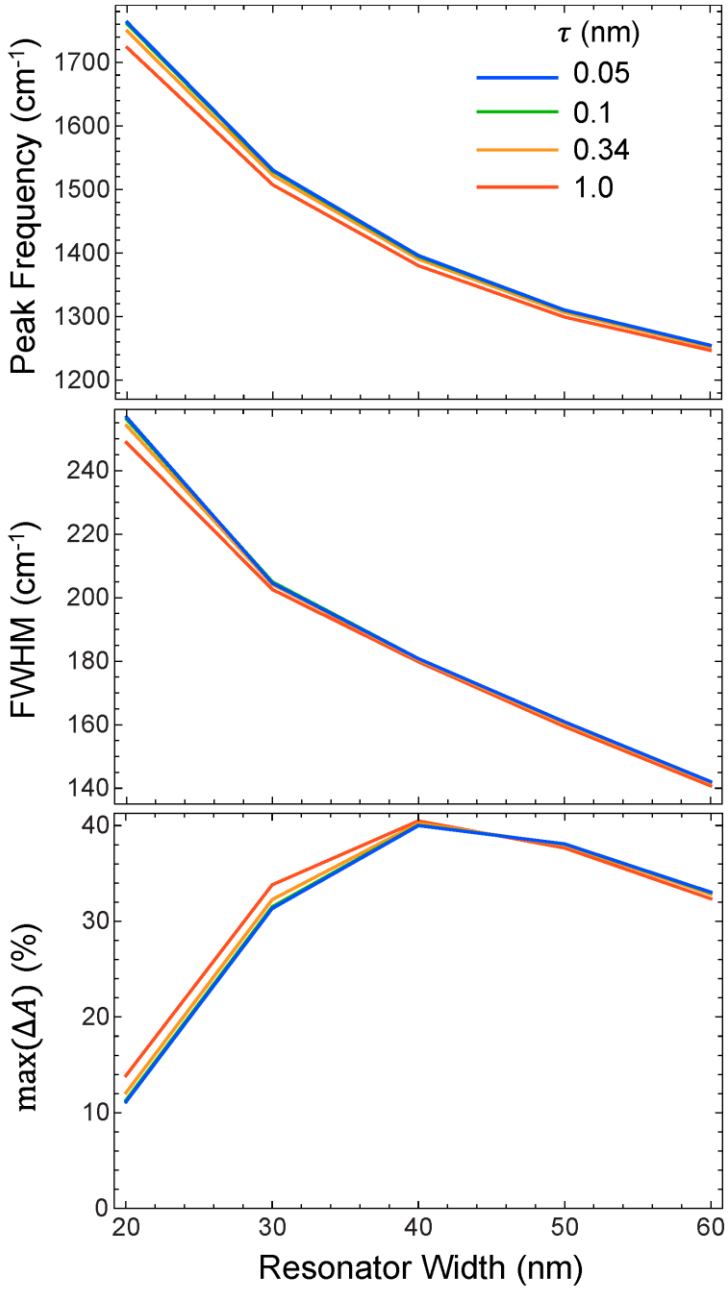

Figure S1: **Convergence of electromagnetic simulations with graphene thickness.** Finite element method (FEM) calculations for plasmon peak frequency (top), line-width (middle), and maximum absorption difference (bottom) of graphene nanoribbons with varying width under

normal incidence. Four different thicknesses of graphene (τ = 0.05, 0.1, 0.34, and 1.0 nm) are investigated. The calculations for τ = 0.1 nm and 0.05 nm are almost identical, assuring that the simulations converge to $\tau \rightarrow 0$ limit. For all cases, the carrier concentration is 1.42×10^{13}cm^{-2}.

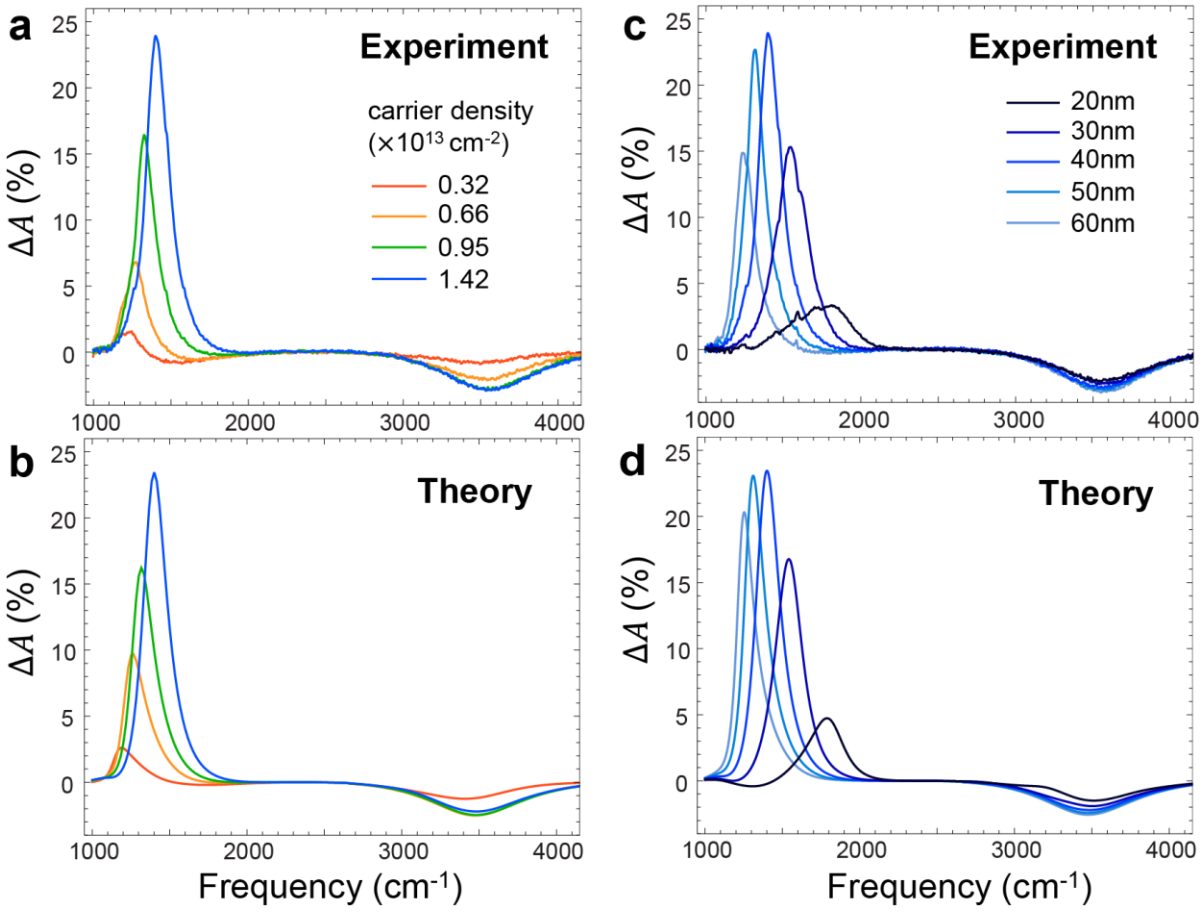

Figure S2: **Comparison between experimental and theoretical absorption spectra.** (a) Experimental and (b) theoretical change in absorption with respect to the absorption at the charge neutral point (CNP) in 40nm wide graphene nanoresonators at various doping levels. (c) Experimental and (d) theoretical absorption difference spectra with the carrier concentration of 1.42×10^{13}cm^{-2}. The width of the resonators varies from 20 to 60nm.

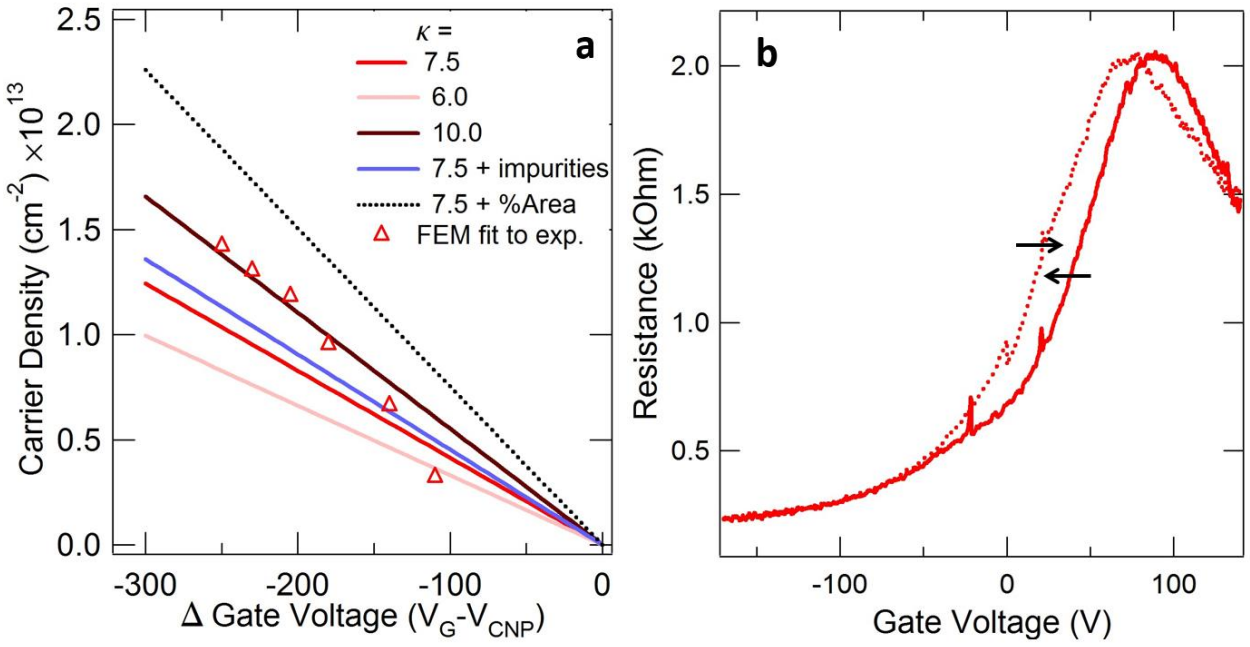

Figure S3: **Carrier density and resistance versus back gate voltage.** (a) Theoretical (lines) carrier density dependence on gate bias for a graphene FET device on a 1 μm thick SiN_x membrane with dielectric properties spanning those reported in literature.[15] The blue line indicates a graphene/SiN_x device that includes estimated doping effects due to atmospheric and substrate impurities that have been reported in SiO_2.[7-10] The black dotted line models a graphene/SiN_x device that contains a graphene surface patterned such that 45% of the sheet has been removed and the surface charge is concentrated into a smaller area. The triangles indicate the calculated carrier densities of our device determined by fitting the simulated peak position to the experimental results. (b) Hysteresis effects in graphene/SiN resistance as applied gate bias swept up (dotted line) and down (solid line). For (a, triangles), the CNP was assumed to occur at +80V, halfway between the two hysteric peaks.

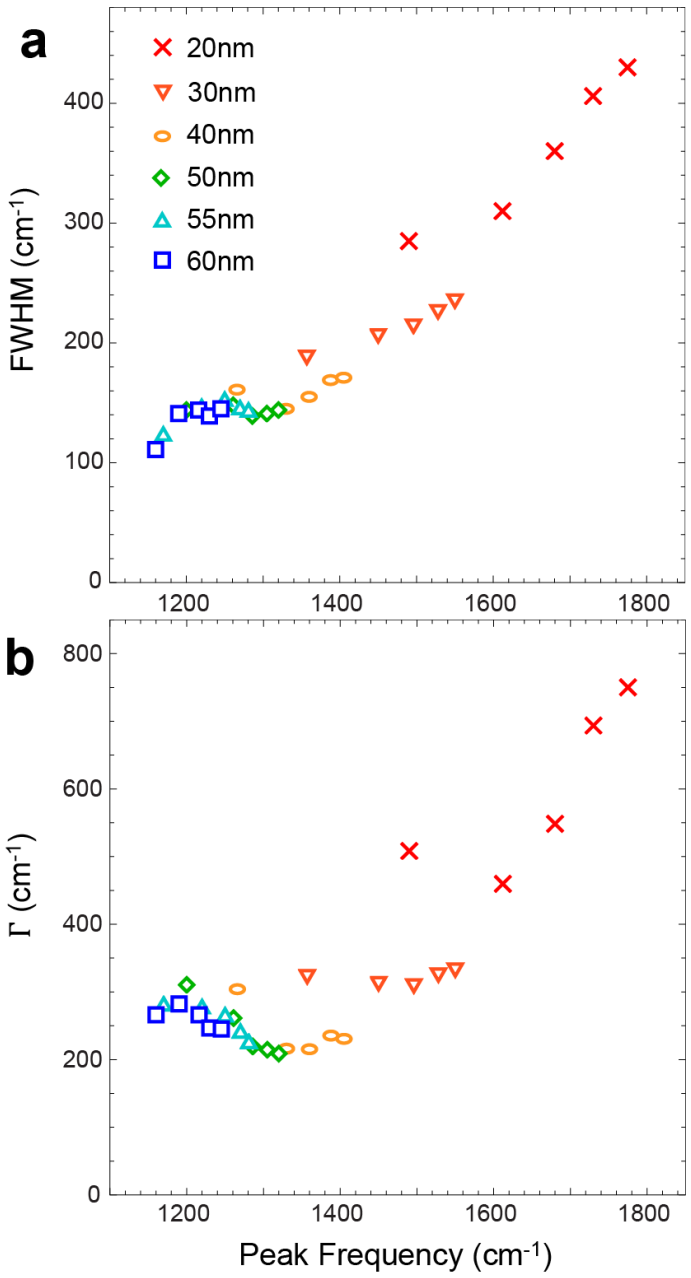

Figure S4: **Peak width and electron scattering rate.** Frequency dependence of (a) the full width at half maximum (FWHM) linewidth of the absorption peaks, and (b) the fitted electron scattering rate. The resonator width ranges from 20 to 60 nm and the carrier density varies from 0.66×10^{13} to 1.42×10^{13}cm^{-2}.

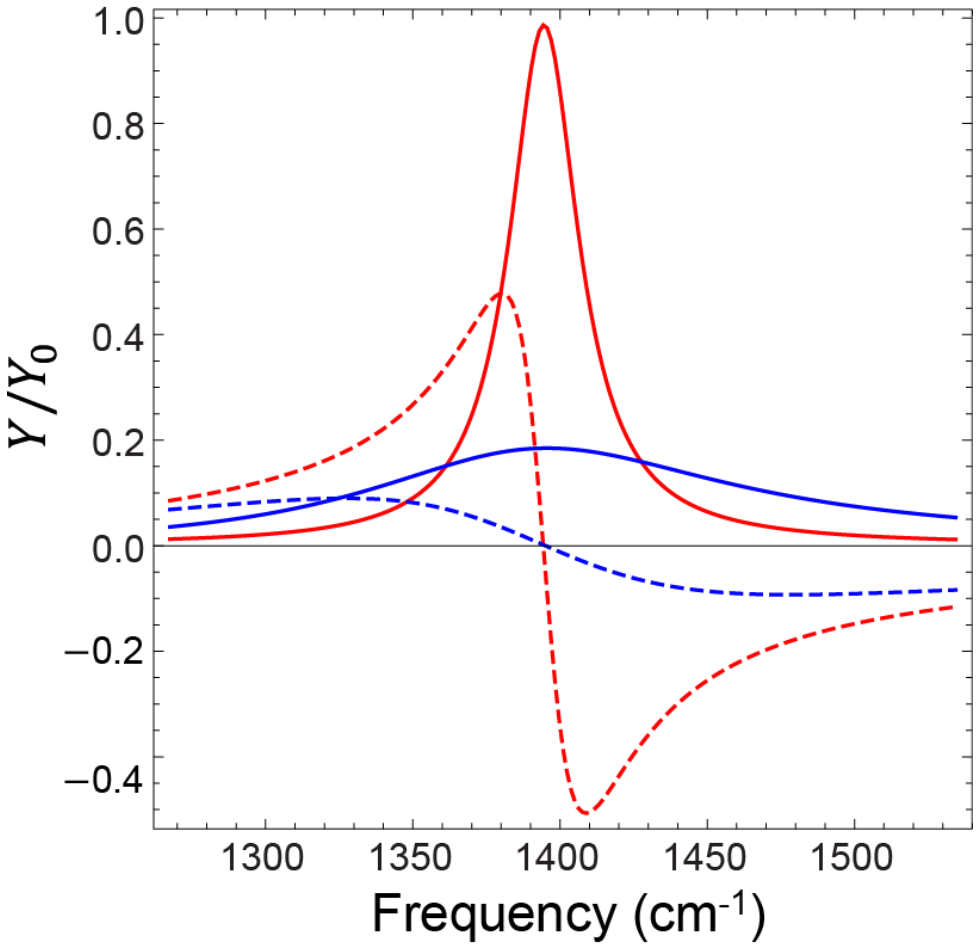

Figure S5: **Surface admittance versus frequency.** Frequency dependence of Re$[Y/Y_0]$ (solid) and Im$[Y/Y_0]$ (dashed) for $\mu = 550$ (blue) and 4,000cm^2/Vs (red). An array of infinitely long graphene nanoribbons (40nm width, 40nm spacing) is assumed. The carrier density is set to 1.42×10^{13}cm^{-2}.

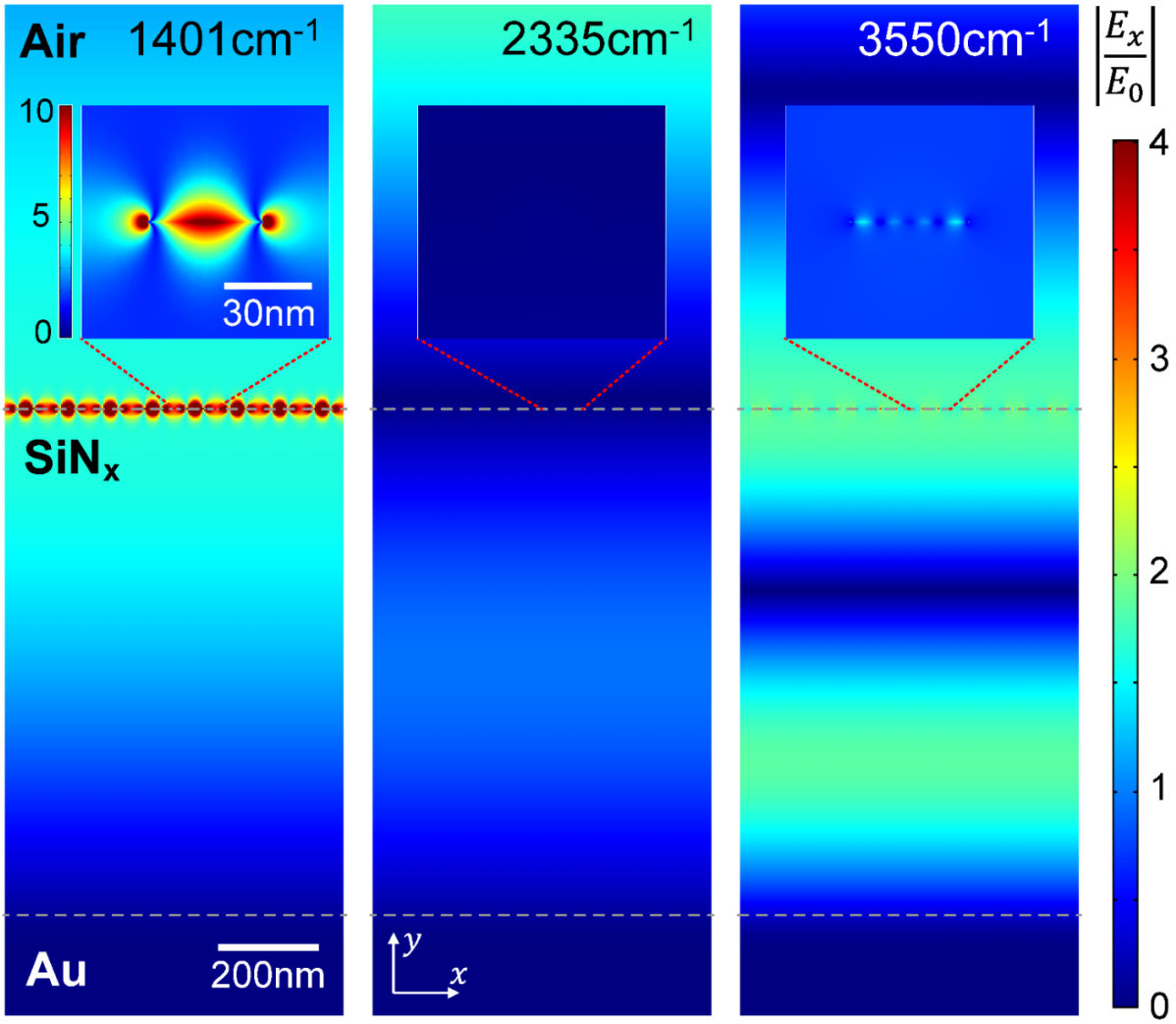

Figure S6: **Electric field distribution.** Theoretical electric field profile of a 40nm graphene nanoresonator with the highest achieved carrier density (1.42×10^{13}cm^{-2}), obtained from an electromagnetic simulation assuming normal incidence. The quarter wavelength condition and plasmon resonance coincide at 1400cm^{-1} (left). At 2335cm^{-1}, the optical thickness of SiN_x is roughly half wavelength, resulting in vanishing electric field at the surface (middle). When the optical thickness of SiN_x becomes three quarters of the wavelength, the surface electric field is maximized again, but the higher order plasmon resonance at this frequency is very weak (right).

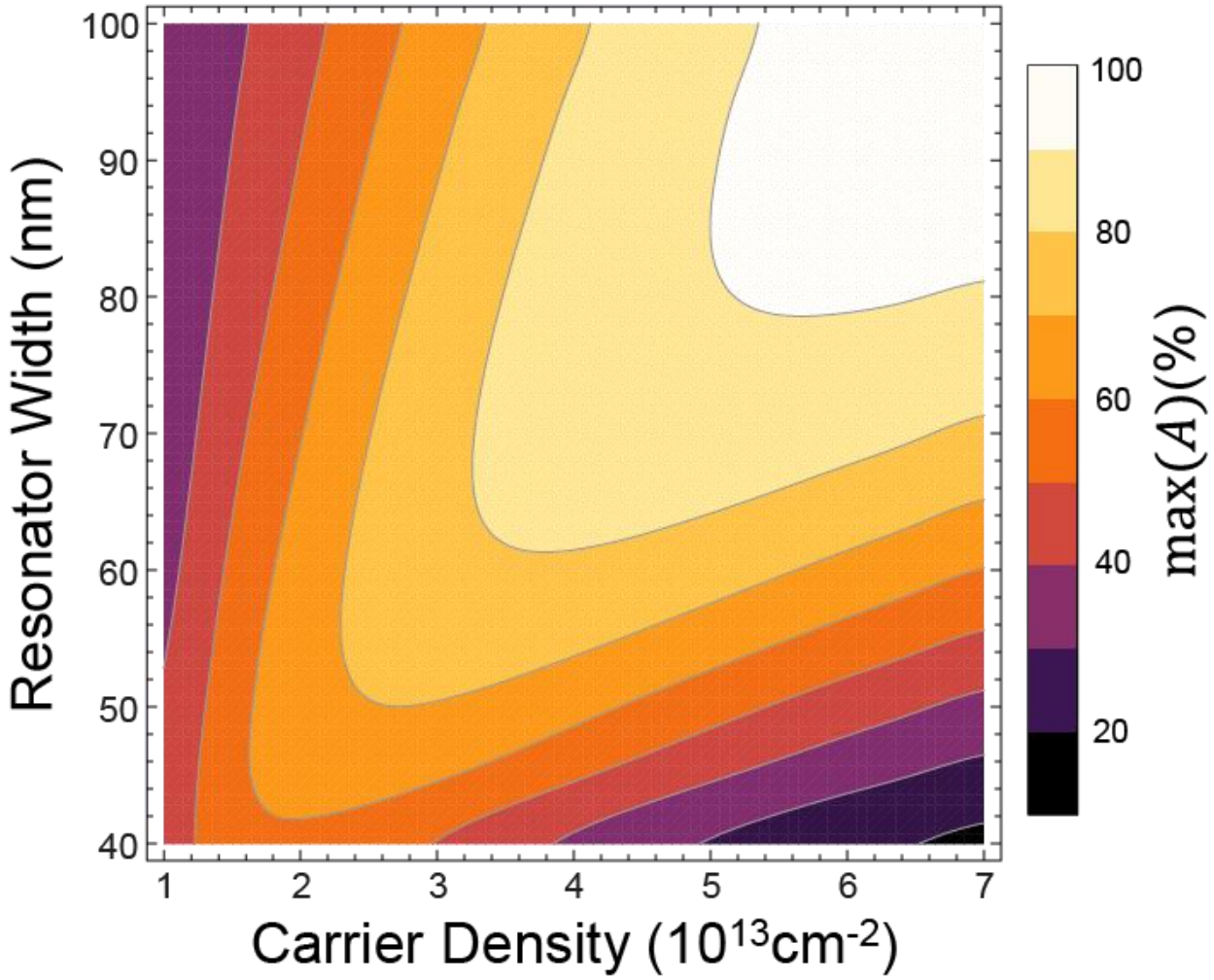

Figure S7: **Peak absorption versus carrier density and resonator width.** Maximum theoretical absorption in a graphene nanoribbon array as a function of the carrier density and the resonator width. The carrier density $1.0-7.0\times10^{13}$cm^{-2}, which is equivalent to the Fermi energy of 0.37−0.98eV. Increasing carrier density leads to better coupling between the incoming light and the graphene plasmons, resulting in stronger plasmon resonance. Therefore, higher doping tends to enhance the absorption performance. The spacing between ribbons is equal to the ribbon width and the SiN_x thickness is set to 1um. The carrier mobility is assumed to be 550cm^2/Vs, and the interaction with graphene optical phonon is considered.[2-4]

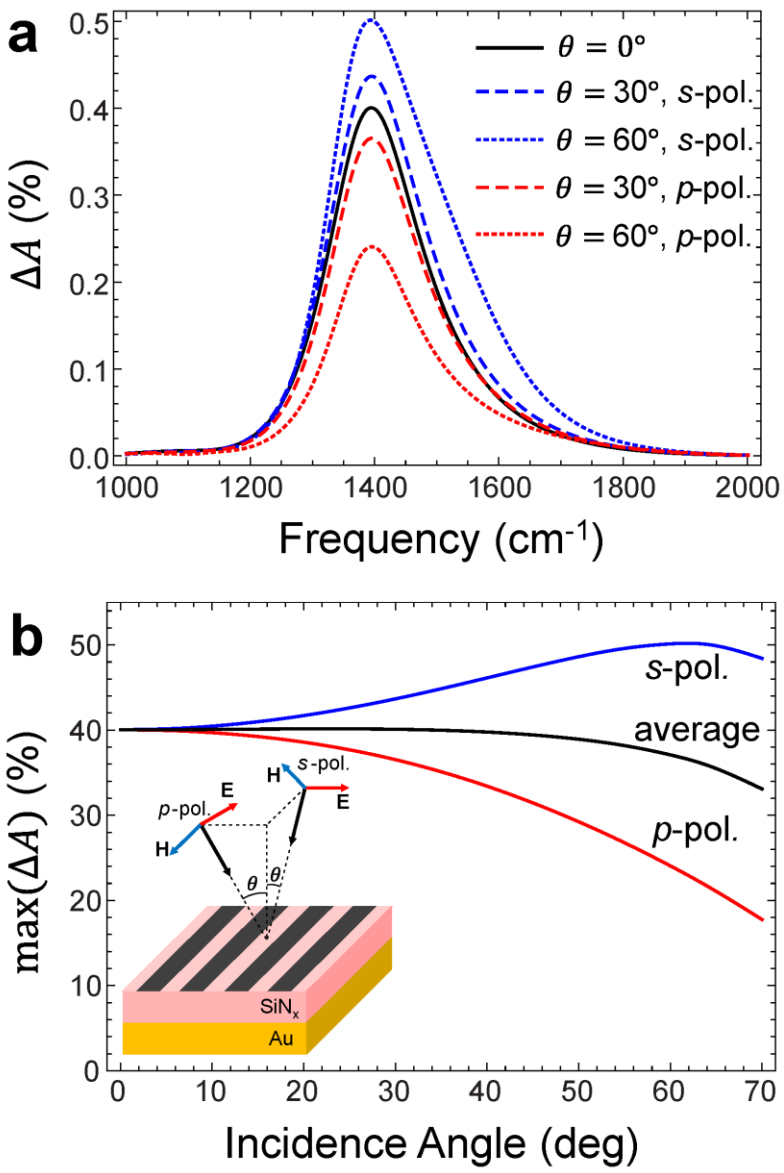

Figure S8: **Incidence angle dependence.** (a) Theoretical change in absorption with respect to the absorption at the charge neutral point in 40nm wide graphene nanoribbons for various incidence angles (θ) and polarizations. (b) Dependence of theoretical maximum absorption difference on the incidence angle for *s*(blue) and *p*(red) polarized illumination. The average maximum absorption (black) does not vary much for $\theta \leq 35°$, which corresponds to the numerical aperture of the objective used in the experiment (N.A. = 0.58). The carrier density and the mobility are assumed to be $1.42\times10^{13}\text{cm}^{-2}$ and $550\text{cm}^2/\text{Vs}$, respectively.

Reference

[1] L. A. Falkovsky and A. A. Varlamov, Eur. Phys. J. B **56**, 281 (2007).
[2] M. Jablan, H. Buljan, and M. Soljacic, Physical Review B **80**, 245435 (2009).
[3] H. Yan, T. Low, W. Zhu, Y. Wu, M. Freitag, X. Li, F. Guinea, P. Avouris, and F. Xia, Nat Photon **7**, 394 (2013).
[4] C.-H. Park, F. Giustino, M. L. Cohen, and S. G. Louie, Physical Review Letters **99**, 086804 (2007).
[5] E. D. Palik, (Elsevier.
[6] G. Cataldo, J. A. Beall, H.-M. Cho, B. McAndrew, M. D. Niemack, and E. J. Wollack, Opt. Lett. **37**, 4200 (2012).
[7] P. L. Levesque, S. S. Sabri, C. M. Aguirre, J. Guillemette, M. Siaj, P. Desjardins, T. Szkopek, and R. Martel, Nano Letters **11**, 132 (2010).
[8] S. Ryu, L. Liu, S. Berciaud, Y.-J. Yu, H. Liu, P. Kim, G. W. Flynn, and L. E. Brus, Nano Letters **10**, 4944 (2010).
[9] H. Wang, Y. Wu, C. Cong, J. Shang, and T. Yu, ACS Nano **4**, 7221 (2010).
[10] H. Xu, Y. Chen, J. Zhang, and H. Zhang, Small **8**, 2833 (2012).
[11] K. Pi, K. M. McCreary, W. Bao, W. Han, Y. F. Chiang, Y. Li, S. W. Tsai, C. N. Lau, and R. K. Kawakami, Physical Review B **80**, 075406 (2009).
[12] S. Thongrattanasiri, I. Silveiro, and F. J. G. de Abajo, Appl Phys Lett **100** (2012).
[13] G. T. Ruck, *Radar cross section handbook* (Plenum Press, New York,, 1970).
[14] R. L. Fante and M. T. McCormack, Antennas and Propagation, IEEE Transactions on **36**, 1443 (1988).
[15] A. Piccirillo and A. L. Gobbi, J Electrochem Soc **137**, 3910 (1990).